Materials Today Bio 15 (2022) 100297

Contents lists available at ScienceDirect

Materials Today Bio

journal homepage: www.journals.elsevier.com/materials-today-bio

PEIGel: A biocompatible and injectable scaffold with innate immune adjuvanticity for synergized local immunotherapy

Zeyu Xiao [a,1], Duo Wang [a,1], Chan Wang [b,1], Zerong Chen [a], Cuiqing Huang [a], Yuan Yang [b], Lin Xie [c], Lulu Zhang [c], Lingling Xu [b], Ming-Rong Zhang [c,**], Kuan Hu [b,c,***], Zhou Li [b,d,****], Liangping Luo [a,*]

[a] The Guangzhou Key Laboratory of Molecular and Functional Imaging for Clinical Translation, The First Affiliated Hospital, Jinan University, Guangzhou, 510632, PR China

[b] CAS Center for Excellence in Nanoscience, Beijing Key Laboratory of Micro-Nano Energy and Sensor, Beijing Institute of Nanoenergy and Nanosystems, Chinese Academy of Sciences, Beijing, 101400, PR China

[c] Department of Advanced Nuclear Medicine Sciences, Institute for Quantum Medical Sciences, Quantum Life and Medical Science Directorate, National Institutes for Quantum Science and Technology, Chiba, 263-8555, Japan

[d] School of Nanoscience and Technology Chinese Academy of Sciences, Beijing, 101400, PR China

ARTICLE INFO

Keywords:
Immune checkpoint therapy
Hydrogel
Polyethylenimine
Immune adjuvant
PD-L1

ABSTRACT

Intratumoral immunotherapeutic hydrogel administration is emerging as an effective method for inducing a durable and robust antitumor immune response. However, scaffold hydrogels that can synergize with the loaded drugs, thus potentiating therapeutic efficacy, are limited. Here, we report a ternary hydrogel composed of polyvinyl alcohol (PVA), polyethylenimine (PEI)–a cationic polymer with potential immunoactivation effects, and magnesium ions–a stimulator of the adaptive immune response, which exhibits an intrinsic immunomodulation function of reversing the immunologically "cold" phenotype of a murine breast tumor to a "hot" phenotype by upregulating PD-L1 expression and promoting M1-like macrophage polarization. PEI hydrogel (PEIGel) encapsulating an immune checkpoint blockade (ICB) inhibitor–anti-PD-L1 antibody (α-PDL1) exhibits synergistic effects resulting in elimination of primary tumors and remote metastases and prevention of tumor relapse after surgical resection. A preliminary mechanistic study revealed a probably hidden role of PEI in modulating the polyamine metabolism/catabolism of tumors to potentiate the immune adjuvant effect. These results deepen our understanding of the innate immune activation function of PEI and pave the way for harnessing PEI as an immune adjuvant for ICB therapy.

1. Introduction

Intratumoral administration of synthetic hydrogels for cancer immunotherapy is emerging as a safe and effective targeted approach for treating many types of tumors [1–3]. Local hydrogel administration could mitigate the adverse effects related to systemic exposure and off-tumor toxicities caused by systemic biodistribution [4,5]. Moreover, intratumoral drug delivery is an attractive approach to increase in situ bioavailability, conferring augmented efficacy for immunotherapies. Compared to immunomodulators injected directly intratumorally, formulations of hydrogels encapsulating immunomodulators show better control over drug pharmacokinetics by extending the release period, thus

* Corresponding author. The Guangzhou Key Laboratory of Molecular and Functional Imaging for Clinical Translation, The First Affiliated Hospital, Jinan University, Guangzhou, 510632, PR China.

** Corresponding author. Department of Advanced Nuclear Medicine Sciences, Institute for Quantum Medical Sciences, Quantum Life and Medical Science Directorate, National Institutes for Quantum Science and Technology, Chiba, 263-8555, Japan.

*** Corresponding authors. CAS Center for Excellence in Nanoscience, Beijing Key Laboratory of Micro-Nano Energy and Sensor, Beijing Institute of Nanoenergy and Nanosystems, Chinese Academy of Sciences, Beijing, 101400, PR China.

**** Corresponding author. CAS Center for Excellence in Nanoscience, Beijing Key Laboratory of Micro-Nano Energy and Sensor, Beijing Institute of Nanoenergy and Nanosystems, Chinese Academy of Sciences, Beijing, 101400, PR China.

E-mail addresses: zhang.ming-rong@qst.go.jp (M.-R. Zhang), kuan.hu@qst.go.jp (K. Hu), zli@binn.cas.cn (Z. Li), tluolp@jnu.edu.cn (L. Luo).

[1] These authors contributed equally to this work.

https://doi.org/10.1016/j.mtbio.2022.100297
Received 13 March 2022; Received in revised form 29 April 2022; Accepted 14 May 2022
Available online 18 May 2022

preventing overactivation of the immune system [6–8] and allowing immunotherapies to be better tolerated for administration of maximally efficacious doses [9–13].

Immune checkpoint blockade (ICB) agents that promote the infiltration of cytotoxic T lymphocytes (CTLs) and restore immune surveillance in cancers by blocking the PD-1/PD-L1 pathway are now widely investigated and applied in the clinical treatment of cancers [8,14–17]. However, ICB agents usually cause unexpected complications or toxicities due to their nonspecific distribution in normal tissues, and these adverse effects pose severe threats to patients' lives [18–20]. In addition, ICB agents induce an effective response in only a minor subset of patients (20%–30%) owing to the immunologically "cold" milieu of many solid tumors [21,22]. To expand the therapeutic potential of ICB in clinical cancer treatment, intratumoral injection of ICB agent-containing hydrogels, either as a single agent or in combination with other therapeutic modalities, e.g., chemotherapy, immunotherapy, or photothermal therapy, has been demonstrated to be an effective method for this purpose [23–35]. Nevertheless, immunotherapeutic scaffold hydrogels that can directly engage in modulating the tumor microenvironment (TME) milieu to promote therapeutic efficacy are largely unmet.

Polyethylenimine (PEI) is a cationic polymer that has been widely applied as a transfection reagent for polynucleotides for decades [36]. In addition to its transportation function, PEI was reported to have immune adjuvant effects to improve the efficacy of vaccines [37]. Moreover, PEI or PEI-based particles have been demonstrated to have a profound ability to directly elicit immune responses by inducing "danger signals" of immune cells and the production of proinflammatory cytokines [38,39]. Although the detailed underlying mechanism of the adjuvanticity of PEI is unclear, the integration of this seductive property of PEI in designing immunotherapeuticals has been intensely pursued, which is believed to promote the unlocking of the mystery of PEI.

In the present study, we reported a ternary PVA-PEI-Mg^{2+} (PEIGel) scaffold hydrogel (PEIGel) with innate immune activation properties for local ICB therapy. PEIGel highlights multiple advantages. First, it can extend the α-PDL1 release to confer durable PD-1/PD-L1 blockade. Moreover, as an immune adjuvant, PEIGel helps induce an immunophenotype favoring ICB, further strengthening the therapeutic efficiency. Notably, this "drug-in-adjuvant" design could mostly reduce the administration dose while maximizing the therapeutic efficacy, which is critical for successful clinical transformation. As a result, α-PDL1/PEIGel significantly outperformed α-PDL1 in suppressing local malignancies and remote metastases of murine breast tumors. Multiplex data supported that PEIGel helped reshape the immunosuppressive TME by upregulating PD-L1 expression and promoting M1 macrophage polarization. More interestingly, a preliminary mechanistic study indicated a potential function of PEI in modulating the polyamine metabolism/catabolism of

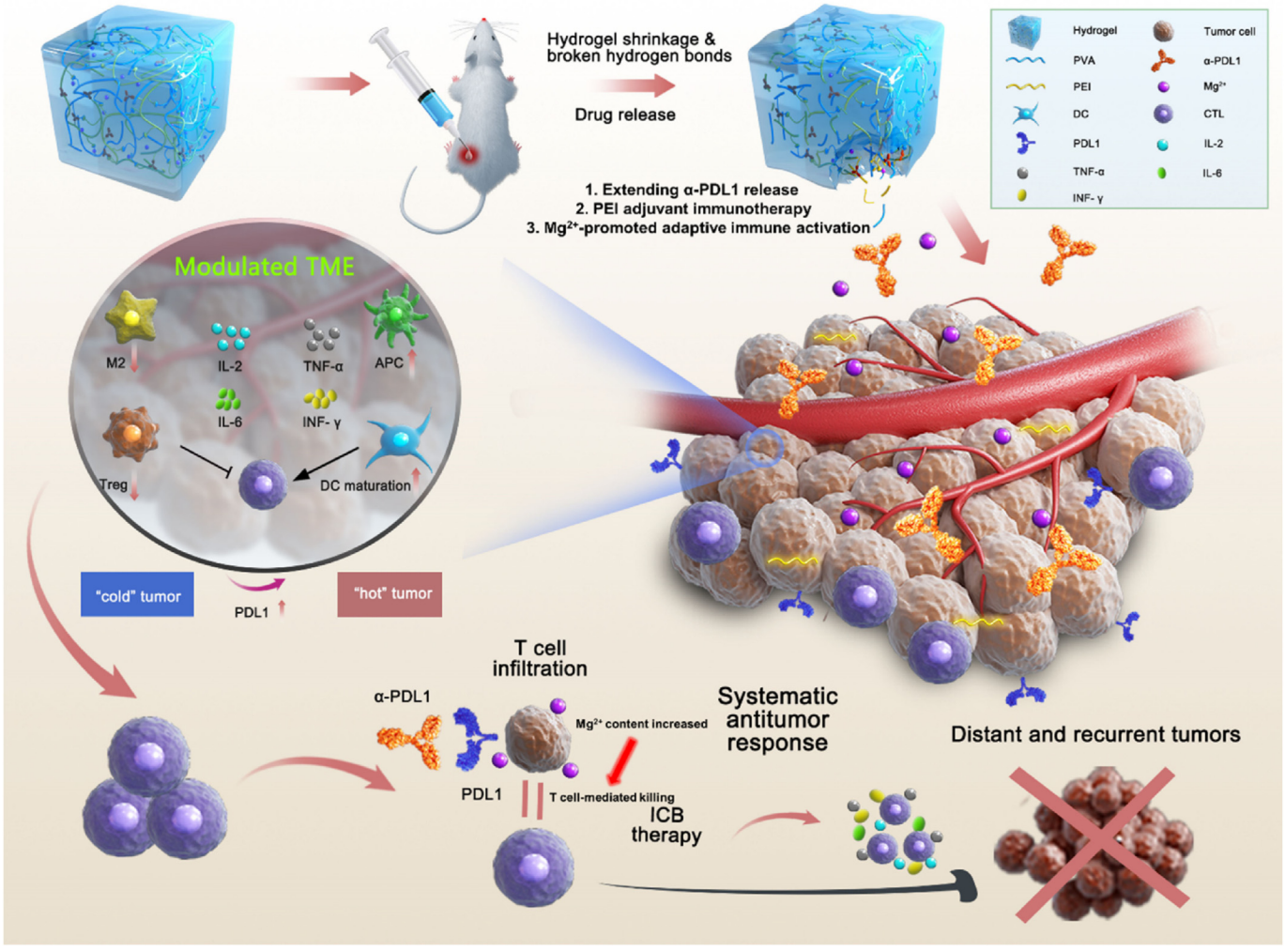

Scheme 1. Schematic illustration of an anti-PD-L1 antibody-loaded PVA-PEI hydrogel (α-PDL1/PEIGel) for boosting and enhancing immune checkpoint blockade (ICB) therapy *via* local administration. PEIGel exerts innate modulatory effects on tumor microenvironment, leading to adjuvant effects that reverse the immunologically "cold" phenotype to a "hot" phenotype by upregulating PDL1 expression and promoting M1-like macrophage polarization. PEIGel encapsulating an anti-PDL1 antibody (α-PDL1) exerts synergistic effects to eliminate primary tumors and remote metastases and to prevent tumor relapse after surgical resection.

the tumor. These studies benefit the design of immunotherapeutic hydrogels for local ICB therapy and deepen our understanding of the multifarious pathways of PEI in modulating the tumor microenvironment (see Scheme 1).

2. Results

2.1. PEIGel encapsulation extends the release of α-PDL1

Adopting the method we reported previously [40], we successfully fabricated an anti-PD-L1 antibody (α-PDL1)-loaded PEIGel (α-PDL1/PEIGel, Fig. 1a). Notably, magnesium cations (Mg^{2+})—a stimulator of the adaptive immune system—were added to the hydrogel to enhance the immunomodulatory activity of the hydrogel [41,42]. The as-prepared α-PDL1/PEIGel was semitransparent and estimated to contain 85% water mass (Fig. 1b). The morphology of the α-PDL1/PEIGel was then investigated *via* cryogenic scanning electron microscopy (cryo-SEM). The lyophilized hydrogel exhibited a porous structure with a 100- to 300-nm pore diameter (Fig. 1c). Energy dispersive spectrometry (EDS) results showed that elements, including C, O, N, Cl, and Mg, were uniformly dispersed in the field (Fig. 1d). Furthermore, Fourier transform infrared spectroscopy (FT-IR) validated that increased hydrogen bonding networks were present in the α-PDL1/PEIGel hydrogel, as evidenced by a widened stretching vibration absorption peak at approximately 3234–3334 cm^{-1} for the α-PDL1/PEIGel compared to the controls (Supplementary Fig. 1**).** The rheological properties of the α-PDL1/PEIGel were assessed by a dynamic mechanical analyzer (DMA). The modulus of the α-PDL1/PEIGel did not change significantly in the temperature range from 20 to 50 °C, suggesting the great thermal stability of the hydrogel (Supplementary Fig. 2). Compared with PVA-based hydrogels, the PEIGel exhibited a profoundly higher viscosity and excellent shear-thinning property, rendering high shape-adaptability to conform to an irregular surgical bed and high flowability to be administered by injection.

Next, we assayed the stability of α-PDL1/PEIGel. The release of α-PDL1 from the PEIGel was first assessed in glass bottles. We observed a stable, sustainable release of α-PDL1 from the PEIGel during the 4 weeks of monitoring. At the endpoint, approximately 20% of the initial α-PDL1 was detected in the buffer, without apparent hydrogel deformation compared to the hydrogel at the starting point (Fig. 1e and Supplementary Fig. 3). Then, in vivo drug release was further investigated *via* an IVIS spectrum system. We employed fluorophore AF647-labeled α-PDL1 (excitation: 670 nm) as a surrogate of α-PDL1 to enable fluorescent detection. Confocal microscopy showed that AF647-α-PDL1 was evenly distributed in the PEIGel scaffold (Supplementary Fig. 4). AF647-α-PDL1/PEIGel was injected into subcutaneous tumors. Simultaneously, an equivalent amount of AF647-α-PDL1 in solution was administered in a parallel cohort as a control. In the mice injected with AF647-α-PDL1, the fluorescence had almost disappeared from the injection site at 7 days after injection. In stark contrast, in mice injected with AF647-α-PDL1/PEIGel, over 50% of the fluorescence was still present at the injection site on day 28 (Fig. 1f and g). These results suggested that PEIGel significantly prolonged the release of α-PDL1.

2.2. Extended release of α-PDL1 boosts antitumor effects on primary tumors

The inhibitory efficacy of α-PDL1/PEIGel on tumor growth was first evaluated in a 4T1 allograft tumor model (Fig. 2a). After 14 days of treatment, the tumor volume of mice in the α-PDL1/PEIGel group (Fig. 2b and c) was significantly smaller than that of mice in the control group. Of note, all mice (5 in 5) in the α-PDL1/PEIGel–treated group (Fig. 2d) survived to day 44, while only one mouse survived (1 in 5) in the α-PDL1–treated group on the same day. Notably, PEIGel treatment prolonged the survival of mice compared to control treatment, implying that PEIGel exerts potential inhibitory effects on tumor growth (Fig. 2b and d).

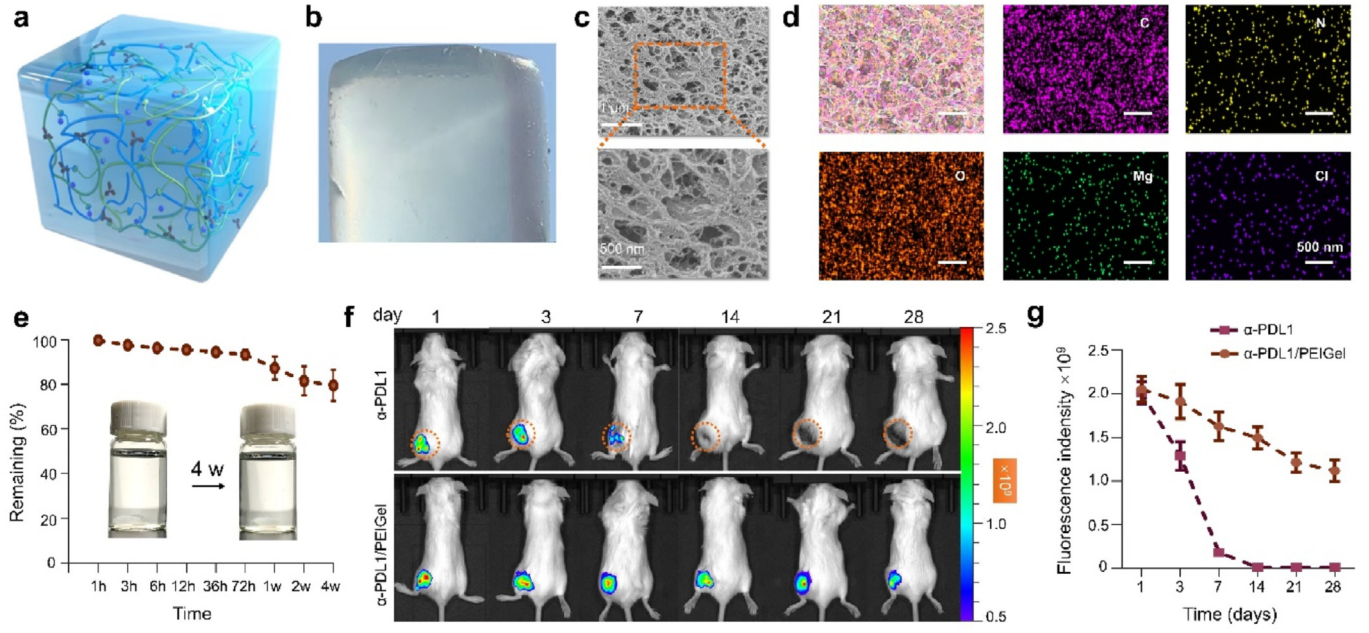

Fig. 1. Preparation and characterization of the α-PDL1/PEIGel. a A model diagram of the PEIGel system. b Representative photographs shows that PEIGel is transparent. c Cryo-SEM images of the α-PDL1/PEIGel at different magnifications (100 × , top; 200 × , bottom), and the pore diameter was calculated to be 100–300 nm d Elemental mapping images of the α-PDL1/PEIGel (scale bar = 500 nm). Carbon (C) is indicated in magenta, nitrogen (N) is indicated in yellow, oxygen (O) is indicated in orange, magnesium (Mg) is indicated in green, and chlorine (Cl) is indicated in purple. e *In vitro* release kinetics of anti-PDL1 from the α-PDL1/PEIGel in 0.01 M PBS buffer (pH 7.4) for 4 weeks, $n = 3$ biologically independent samples per group. f Release kinetics of AF647-α-PDL1 from the PEIGel in a 4T1 allograft murine model over 28 days (intratumoral injection). g Semiquantitative analysis of AF647-α-PDL1 released from the PEIGel over 28 days based on fluorescence intensity, $n = 3$ biologically independent mice per group. Data are shown as the mean ± SD. Statistical analysis was performed by a two-tailed Student's *t*-test. $^{*}P < 0.05$, $^{**}P < 0.01$, $^{***}P < 0.001$, $^{****}P < 0.0001$.

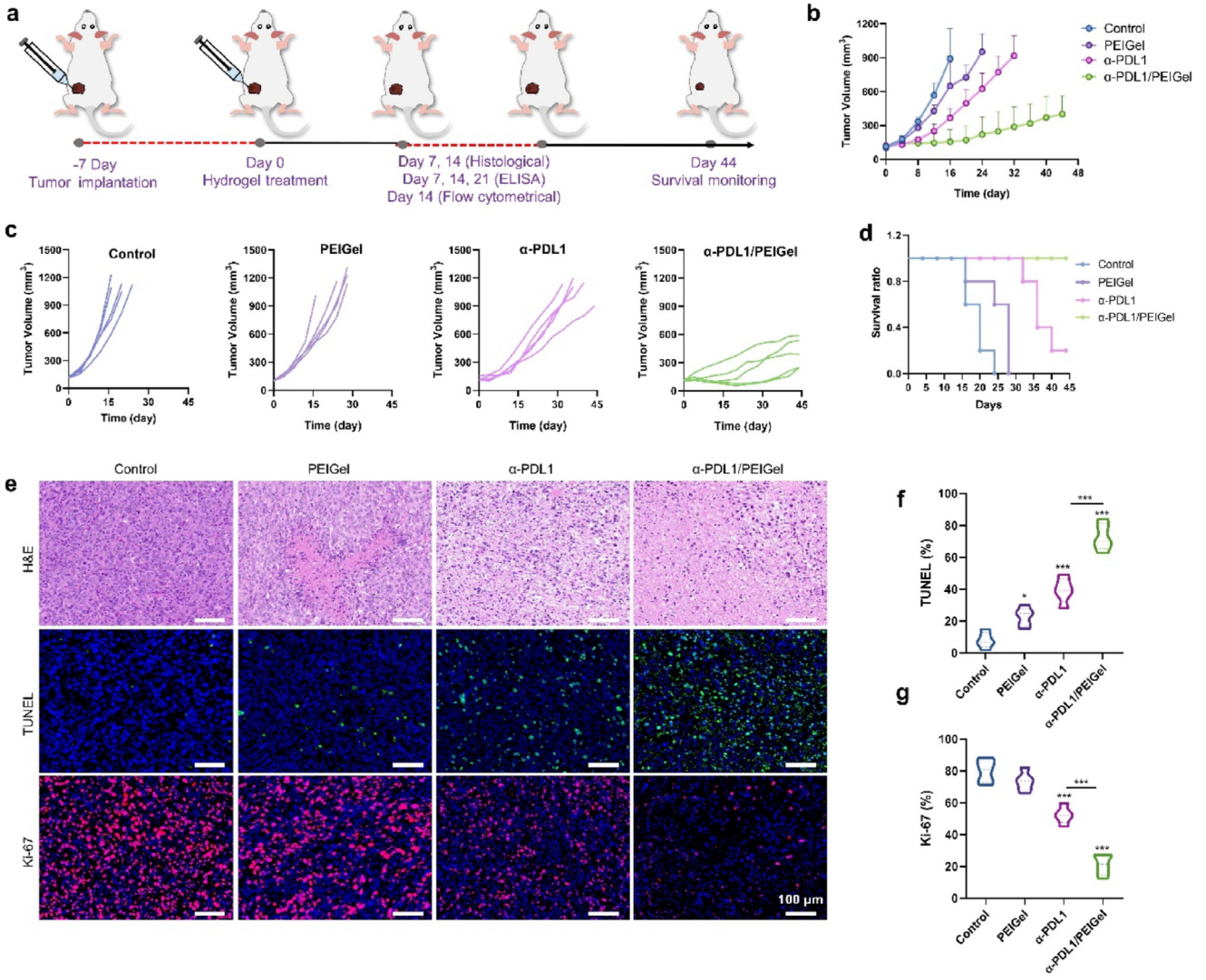

Fig. 2. Antitumor efficacy of the α-PDL1/PEIGel in a 4T1 allograft murine model. a Schematic diagram of the animal experiment. 4T1 tumor-bearing mice were intratumorally injected with 100 μL PBS, PEIGel, α-PDL1 or α-PDL1/PEIGel (dose equivalent to 100 μg α-PDL1) on day 0, and serum was collected on days 7, 14 and 21 for ELISA detection of IL-2, IL-6, TNF-α and IFN-γ. b Tumor growth curves of 4T1 tumor-bearing mice treated with PBS, PEIGel, α-PDL1 or α-PDL1/PEIGel (n = 5) for 44 days, with an endpoint tumor volume of 1000 mm^3 used as a surrogate for mortality. c Individual tumor volumes of the 4T1 allograft model mice given various treatments, n = 5 biologically independent mice per group. d Kaplan–Meier survival analysis of 4T1 tumor-bearing mice. e Cell apoptosis in tumors from different treatment groups was detected *via* H&E staining, a TUNEL assay and Ki67 immunofluorescence analysis. Cell nuclei were stained with 4′,6-diamidino-2-phenylindole (DAPI, blue fluorescence). Apoptotic cells were identified by green fluorescence, and Ki67 was identified by red fluorescence; scale bar = 100 μm. Semiquantitative analysis of the $TUNEL^+$ percentage and g Ki67 expression in tumors from different treatment groups, n = 5. Data are presented as the mean ± SD. Statistical analysis was performed by one-way ANOVA with Tukey's post-hoc test (f, g). The log-rank test was used to compare survival among the groups (b). -*$P < 0.05$, **$P < 0.01$, ***$P < 0.001$, ****$P < 0.0001$.

To verify the tumor inhibitory effects, further anatomical histochemical analysis was performed. As shown by hematoxylin and eosin (H&E) staining (Fig. 2e), active proliferation of cancer cells was observed in the control group, PEIGel group and even α-PDL1 group, while in the α-PDL1/PEIGel group, purple staining was significantly reduced, indicating massive cancer cell death. Moreover, as observed with a terminal deoxynucleotidyl transferase dUTP nick end labeling (TUNEL) assay (Fig. 2e and f), strong green fluorescence could be detected in tumor tissues from the α-PDL1/PEIGel group, indicating massive apoptosis of 4T1 cancer cells. More specifically, the number of TUNEL-positive cells in the α-PDL1/PEIGel group (~70%) was higher than that in the control group (~10%) according to semiquantitative analysis. Ki67 was also utilized to evaluate the proliferation of cancer cells. As shown in Fig. 2e and g, the Ki67-positive areas in the α-PDL1/PEIGel group were reduced by ~60% and 70% compared to those in the α-PDL1 group and PEIGel group, respectively, validating that tumor growth was significantly inhibited by local administration of α-PDL1/PEIGel.

2.3. *PEIGel synergizes with α-PDL1 to reshape the TME*

To gain insight into the antitumor mechanism of α-PDL1/PEIGel, we next performed an enzyme-linked immunosorbent assay (ELISA) analysis. As shown in Fig. 3a–d, after local α-PDL1/PEIGel administration, the levels of cytokines, including interleukin-2 (IL-2), interleukin-6 (IL-6), tumor necrosis factor alpha (TNF-α) and interferon-gamma (IFN-γ), in the blood were all significantly increased, indicating the activation of a systemic antitumor immune response in the mice. Strikingly, the cytokine levels of mice treated with PEIGel alone on day 14 were also significantly increased compared to those of the mice in the control group and α-PDL1 group. Of note, the cytokine levels of mice in the PEIGel and

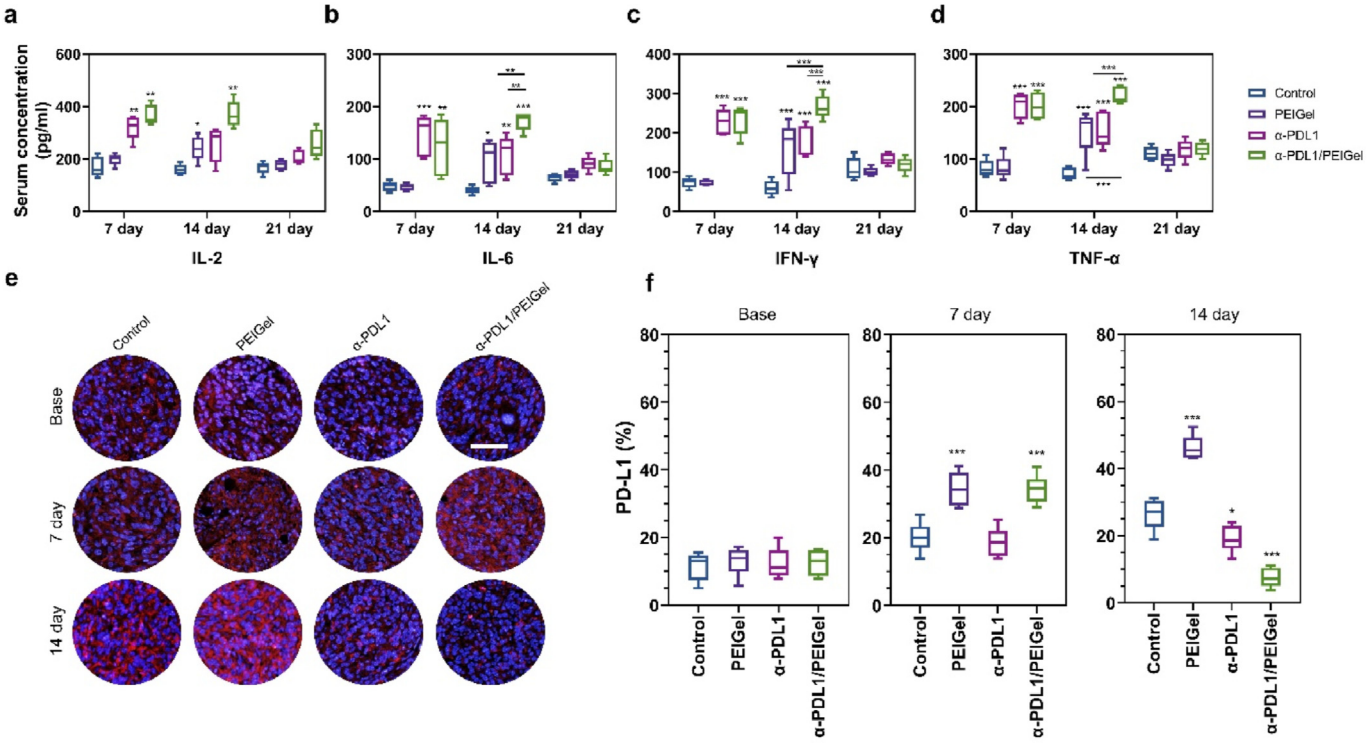

Fig. 3. α-PDL1/PEIGel inflamed the tumor microenvironment and enhanced systemic antitumor immune responses. a-d The levels of cytokines, including IL-2, IL-6, IFN-γ, and TNF-α, in the serum of mice treated with PBS, the PEIGel, α-PDL1 or the α-PDL1/PEIGel (intratumoral injection of an amount equivalent to 100 μg α-PDL1) on days 7, 14 and 21, $n = 5$ biologically independent mice per group. e Immunofluorescence analysis of PDL1 expression in tumors from different treatment groups at baseline and on days 7 and 14 ($n = 5$). Nuclei were stained with DAPI (blue fluorescence), and PD-L1 was identified by red fluorescence; scale bar = 100 μm i Semiquantitative analysis of PD-L1 expression at baseline and on days 7 and 14, $n = 5$. Data are presented as the mean ± SD. Statistical analysis was performed by one-way ANOVA with Tukey's post-hoc test. *$P < 0.05$, **$P < 0.01$, ***$P < 0.001$, -****$P < 0.0001$.

α-PDL1/PEIGel groups on day 14 were maintained or even increased compared to those on day 7. In contrast, the cytokine levels in mice in the α-PDL1 group showed a remarkable decrease from day 7 to day 14.

As a "cold" tumor phenotype with low PDL1 expression, 4T1 tumors often exhibit an immunosuppressive TME with low cytotoxic T lymphocytes (CTL) and high regulatory T (T_{reg}) cell infiltration [25]. It is thus crucial to "heat" the tumor for effective antitumor immunotherapy. Increasing evidence has shown that the expression level of PDL1 in tumors is closely associated with the efficacy of ICB-based cancer immunotherapy [43,44]. Upregulating PDL1 expression by chemical or physical treatments, such as mild photothermal irradiation, has been demonstrated to be an effective approach to potentiate immunologically "cold" tumors to respond to ICB [29]. Following the observation of the immune modulation effects of PEIGel, we then sought to inspect whether PEIGel modulates the PDL1 expression level of tumors. According to an immunofluorescence analysis of PDL1 expression in 4T1 tumors, local administration of PEIGel effectively enhanced PDL1 expression and improved the heterogeneity of PDL1 expression (Fig. 3e). A similar elevation in PDL1 expression was also observed in mice treated with α-PDL1/PEIGel on day 7. This unique function of the PEIGel could support CTL infiltration during the early stage of treatment. However, in mice treated with α-PDL1 or the α-PDL1/PEIGel, most of the 4T1 tumor cells underwent apoptosis, leading to drastically decreased expression of PDL1 at the end of the treatment period (Fig. 3i). The above results were further confirmed by western blot analysis (Supplementary Fig. 5).

To assess whether local α-PDL1/PEIGel administration improves the tumor infiltration of CTLs, we then performed immunofluorescence analysis. The infiltration of $CD3^+$ and $CD8^+$ T cells into 4T1 tumors treated with α-PDL1/PEIGel was significantly increased compared to that in tumors given other treatments (Fig. 4a and Supplementary Fig. 6a), suggesting the induction of robust infiltration of CTLs and other types of T cells. For tumors treated with PEIGel, although the $CD3^+$ cell level showed no significant increase compared to that in the control group, there was a noticeable elevation in $CD8^+$ T-cell numbers (Supplementary Fig. 6b and c), indicating that PEIGel could induce CTL accumulation to reprogram the suppressive TME (Supplementary Fig. 7).

To dissect the cellular and molecular changes among immune cell subsets after intratumoral administration of α-PDL1/PEIGel, we evaluated the composition and activation status of leukocytes in tumors. As shown in Supplementary Fig. 8a and b, after α-PDL1/PEIGel treatment, the percentage of infiltrated $CD3^+$ T cells in 4T1 tumors was increased significantly. Moreover, as shown in Fig. 4b–d and 4f-4h, local α-PDL1/PEIGel administration effectively increased the percentages of $CD3^+CD8^+$ T cells and IFN-γ^+CD8^+ T cells, while the percentage of $CD4^+FOXP3^+$ T_{reg} cells was greatly decreased. A slight increase in $CD3^+CD8^+$ T cells was also detected in the PEIGel group on day 14. An increase in $CD80^+CD86^+$ antigen-presenting cells was observed in all three treatment groups (Supplementary Fig. 8c and d) and demonstrated that the immunosuppressive environment was efficiently alleviated. Moreover, the percentage of cells expressing CD206 (an indicator of M2 macrophages) in the PEIGel group decreased to 37.1% in contrast with that in the control group (42.1%), indicating that PEIGel may efficiently induce macrophage polarization from an M2 phenotype to an M1 phenotype (Fig. 4e and i). This effect was also confirmed by the *in vitro* co-culture model of PEIGel and RAW246.7 cells (Supplementary Fig. 9).

2.4. PEIGel synergizes with α-PDL1 to eliminate metastases

Tumor metastasis is a common phenomenon during cancer progression and is a major cause of tumor-associated death. Immunotherapies that produce systemic antitumor immune responses are highly promising treatment modalities to eliminate both primary tumors and metastatic

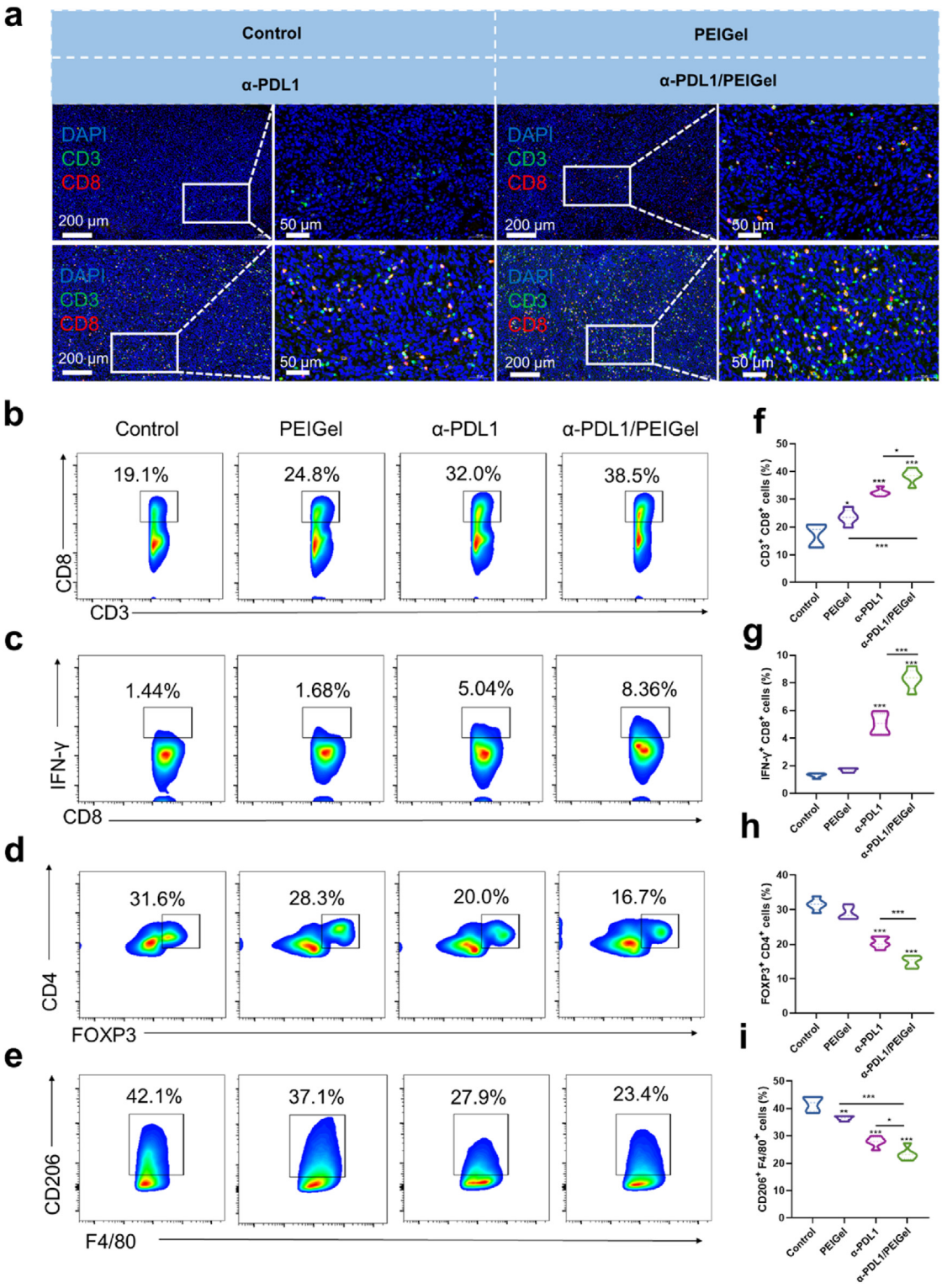

Fig. 4. Antitumor immunity induced by the α-PDL1/PEIGel in a 4T1 allograft murine model. a Infiltration of T lymphocytes into tumors from different treatment groups. Nuclei were stained with DAPI (blue fluorescence), $CD3^+$ cells were identified by green fluorescence, and $CD8^+$ cells were identified by red fluorescence; scale bar = 200 μm. 4T1 tumor-bearing mice were intratumorally injected with 100 μL PBS, PEIGel, α-PDL1 or α-PDL1/PEIGel (dose equivalent to 100 μg α-PDL1) on day 0, and the subcutaneously transplanted tumors were removed on day 14 for immunofluorescence and flow cytometric analysis. a Infiltration of T lymphocytes into tumors from different treatment groups. Nuclei were stained with DAPI (blue fluorescence), $CD3^+$ cells were identified by green fluorescence, and $CD8^+$ cells were identified by red fluorescence; scale bar = 200 μm and 50 μm. a-e Flow cytometric analysis and f-i quantitative analysis of $CD8^+$ T cells after gating on $CD45^+CD3^+$ cells, IFN-γ^+ T cells after gating on $CD45^+CD3^+CD8^+$ cells, T_{reg} cells after gating on $CD4^+FOXP3^+$ cells, and M2-like macrophages ($CD206^+$) after gating on $CD45^+CD11b^+F4/80^+$ cells; $n = 5$ biologically independent mice per group. Data are presented as the mean ± SD. Statistical analysis was performed by one-way ANOVA with Tukey's post-hoc test. $^*P < 0.05$, $^{**}P < 0.01$, $^{***}P < 0.001$, $^{****}P < 0.0001$.

tumors. To evaluate the antimetastatic efficacy of the α-PDL1/PEIGel, we established a 4T1 tumor metastasis murine model for an antimetastatic study (Fig. 5a). After 16 days of treatment, local α-PDL1/PEIGel administration successfully inhibited the growth of both primary tumors and distant tumors (Supplementary Fig. 10-11 and Fig. 5b). As expected, intratumoral injection of α-PDL1 also mitigated the growth of distant tumors. However, the efficacy was much weaker than that achieved with α-PDL1/PEIGel. Interestingly, PEIGel administration also showed some ability to delay distant tumor growth (Fig. 5b).

As shown in Supplementary Fig. 12a and 12b, the Ki67-positive areas in the α-PDL1/PEIGel group were reduced significantly compared to those in the α-PDL1 group and PEIGel group, validating that tumor growth was significantly inhibited by local administration of α-PDL1/PEIGel. Furthermore, ELISAs were used to evaluate cytokines, including IL-2, IL-6, TNF-α and IFN-γ, in the tumor. The results showed that the levels of all cytokines were significantly increased in all treated groups, revealing the order α-PDL1/PEIGel > α-PDL1 > PEIGel > control (Fig. 5c–f). This suggests that local administration can effectively induce a systemic antitumor immune response, resulting in the elimination of tumor metastases.

The tumor immune status in distant tumors was further investigated by immunofluorescence analysis. As shown in Fig. 5g and Supplementary Fig. 13, the maximum infiltration of $CD3^+CD8^+$ T cells was detected in distant tumors treated with α-PDL1/PEIGel. Although α-PDL1 treatment alone also elicited robust infiltration of $CD3^+CD8^+$ T cells in distant tumors, the staining intensity was significantly lower (Fig. 5g). We next performed flow cytometric analysis to probe the variations in immune cell subsets in distant tumors after local treatment. As shown in Fig. 5h, j, and Supplementary Fig. 14, local α-PDL1/PEIGel administration significantly increased the percentage of infiltrated $CD8^+$ T cells in the distant tumors, with the percentages of $CD3^+CD8^+$ and IFN-γ^+CD8^+ T cells being increased to 29.6% and 7.04% compared to 12.9% and 2.28% in the control group, respectively. Notably, although local administration of PEIGel failed to promote CTL infiltration, it decreased the percentage of infiltrated $FOXP3^+CD4^+$ T_{reg} cells (28.1%) in distant tumors compared to control treatment (32.7%) (Fig. 5i and k), suggesting a potential role in reprogramming the TME by alleviating immunosuppressive factors.

2.5. PEIGel synergizes with α-PDL1 to prevent primary tumor relapse after surgery

In the clinical treatment of solid tumors, surgical resection alone usually fails to cure advanced-stage cancers due to local relapse caused by conservative surgical resection or remote metastasis. Therefore, surgical resection in combination with other treatment modalities, such as immunotherapy, has been considered an effective regimen to improve patient prognosis and overall survival. To evaluate the utility of the α-PDL1/PEIGel in preventing tumor relapse after surgery, we established a recurrent tumor model with 4T1 tumor-bearing mice and investigated the antirelapse efficacy of the α-PDL1/PEIGel, as indicated in Fig. 6a. The differences in recurrent tumor volumes among the different treatment groups (Fig. 6b−6e) demonstrated that α-PDL1/PEIGel had the best antirelapse efficacy. Specifically, 3 of the 6 mice treated with α-PDL1/PEIGel were cured and showed no detectable tumors on day 30. Furthermore, on the same day, 2 of the 3 recurrent mice showed small tumor volumes of less than 50 mm^3, and only one mouse grew a tumor with a volume over 100 mm^3. In contrast, for mice injected with α-PDL1 in solution locally, the recurrent tumor volumes of 3 of the 6 mice were larger than 100 mm^3 on day 30, and only 1 of the 6 mice was completely cured. These results suggest that PEIGel encapsulation may enhance the antitumor immune response induced by α-PDL1 to inhibit tumor recurrence *via* extended release.

Flow cytometric analysis further confirmed the high infiltration of $CD3^+CD8^+$ T cells in recurrent tumors treated with the α-PDL1/PEIGel (Fig. 6f−6i). In addition, the increase in activated CTLs further suggested the activation of the antitumor immune response and enhancement of immune recognition, as the percentage of IFN-γ^+ $CD8^+$ T cells in recurrent tumors from the α-PDL1/PEIGel group was increased to 12.4% compared to 4.09% in the control group. Therefore, through the sustained release of α-PDL1 from the PEIGel, immune suppression in recurrent tumors can be relieved, efficiently preventing tumor recurrence and regrowth after surgical resection. Based on these results, it was confirmed that local administration of α-PDL1/PEIGel may hold great potential for the clinical treatment of solid tumors by relieving immune suppression and promoting CTL infiltration.

2.6. PEIGel potentially modulated the polyamine metabolism/catabolism of tumors

The above results consistently suggested that PEIGel shows innate immune modulation effects, which can be partly due to the immune adjuvanticity of PEI. Regarding the immune activation function of PEI, although a couple of studies have established possible immune pathways that can be affected by PEI, most of them focus on downstream immune effectors or immune receptors expressed by immune cells. Nevertheless, how PEI influences the fate of tumor cells remains largely unexplored.

The innate polyamines of mammals, usually referred to as putrescine, spermidine and spermine, are highly charged, polycationic alkylamines, which are fundamental substrates in maintaining cell growth and survival, and their depletion leads to cytostasis [45–47]. Increasing evidence has shown that polyamine metabolism is dysregulated in cancers, with elevated polyamine levels characterizing malignancies [48–50]. Moreover, increasing knowledge supports the existence of interplay between polyamine metabolism and other tumor-driving pathways [51].

In this context, we investigated whether PEIGel is involved in modulating polyamine metabolism/catabolism in 4T1 tumors [52]. We first evaluated the polyamine levels in 4T1 tumors following 14 days of treatment using ultra-performance liquid chromatography (UPLC) analyses based on the method reported previously [53,54] (Fig. 7a). As expected, we observed a significant depletion of intratumoral spermine levels led by the PEIGel and α-PDL1/PEIGel treatment, while α-PDL1 alone caused no changes in the spermine level (Fig. 7b–d). Furthermore, the spermine-to-spermidine ratio was significantly decreased following PEIGel or α-PDL1/PEIGel treatment (Fig. 7e), suggesting an upregulation of polyamine catabolism or downregulation of polyamine synthase activity [53–55]. In addition, the expression levels of two critical polyamine catabolism enzymes, spermidine/spermine N^1-acetyltransferase 1 (SSAT) and spermine oxidase (SMOX), showed notable increases following PEIGel and α-PDL1/PEIGel treatment (Fig. 7f–h). These results preliminarily indicated that PEI is a potential SSAT inducer that may interrupt polyamine catabolism/metabolism in 4T1 cells and promote immunogenic cell death of cancer cells (Fig. 7i). Currently, the in-depth investigation of the correlation between PEI's immune adjuvanticity and its polyamine modulation ability is ongoing.

2.7. PEIGel exhibits good biosafety

After confirming its broad utility in eliminating both primary tumors and metastatic tumors in murine tumor models, we sought to assay the biocompatibility of the α-PDL1/PEIGel, a critical analysis before its utilization in clinical research. First, we confirmed the low cytotoxicity of PEIGel by co-culture with AML-12 and HUVECs cells (Supplementary Fig. 15). Then, hematological analysis was performed to monitor the potential toxicity to blood cells. As suggested in Supplementary Fig. 16 and Supplementary Table S1, local α-PDL1/PEIGel administration did not induce obvious acute toxicity since the numbers of white blood cells (WBCs), red blood cells (RBCs) and platelets (PLTs) and the level of hemoglobin (HGB) in routine blood assays were maintained in the corresponding normal range. Moreover, biochemical analysis of the blood revealed that the levels of albumin (ALB), globulin (GLB), alanine aminotransferase (ALT), aspartate aminotransferase (AST), lactate dehydrogenase (LDH), blood urea (urea), cystatin C (Cys C) and creatinine

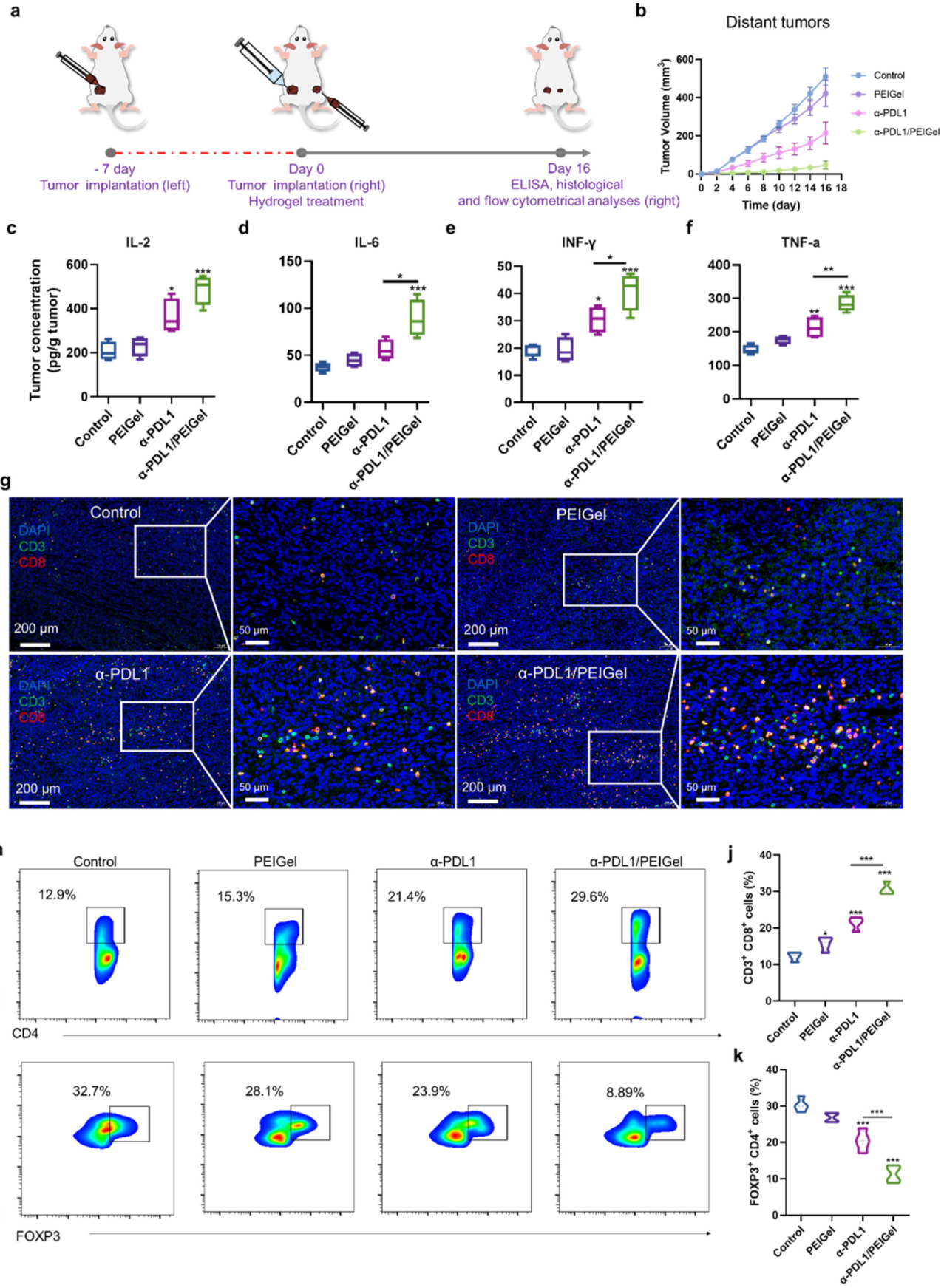

(caption on next page)

Fig. 5. Antitumor efficacy of the α-PDL1/PEIGel in a metastatic tumor model. a Schematic diagram of the animal experiment. Intratumoral injection of 100 μL PBS, PEIGel, α-PDL1 or α-PD-L1/PEIGel (dose equivalent to 100 μg anti-PD-L1) on day 0. b Average tumor volumes of metastatic tumors in 4T1 tumor-bearing mice treated with PBS, PEIGel, α-PDL1 or α-PD-L1/PEIGel (intratumoral injection, dose equivalent to 100 μg anti-PDL1, $n = 4$). c-f Distant tumor cytokine levels in different treatment groups on day 16 ($n = 4$). g Nuclei were stained with DAPI (blue fluorescence), $CD3^+$ cells were identified by green fluorescence, and $CD8^+$ cells were identified by red fluorescence; scale bar = 200 μm and 50 μm. h-i Flow cytometric analysis and j-k semiquantitative analysis of $CD8^+$ T cells after gating on $CD45^+CD3^+$ cells, and T_{reg} cells after gating on $CD4^+FOXP3^+$ cells; $n = 4$ biologically independent mice per group. Data are presented as the mean ± SD. Statistical analysis was performed by one-way ANOVA with Tukey's post-hoc test. $^*P < 0.05$, $^{**}P < 0.01$, $^{***}P < 0.001$, $^{****}P < 0.0001$.

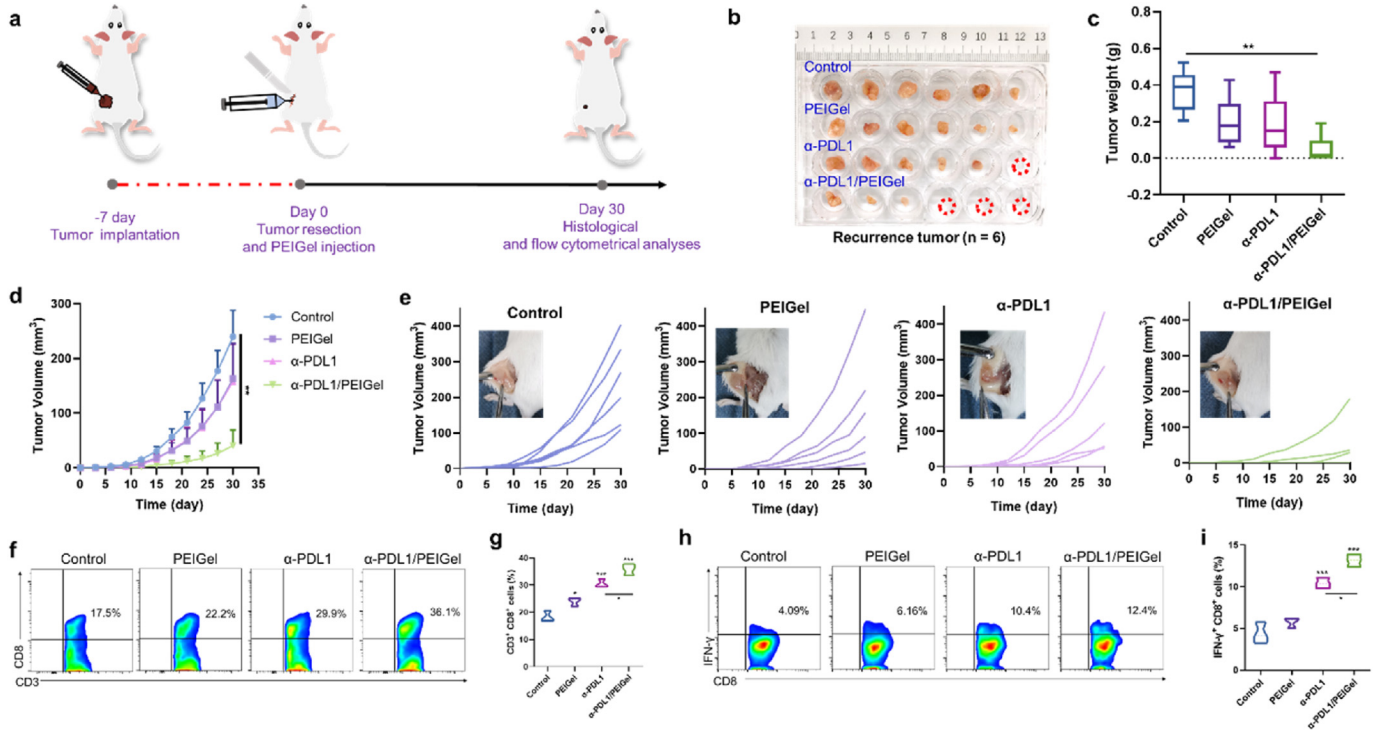

Fig. 6. Antitumor efficacy of the α-PDL1/PEIGel in a recurrent tumor model. a Schematic diagram of the animal experiment. 4T1 tumors were partly resected on day 0, and then 100 μL PBS, PEIGel, α-PDL1 or α-PDL1/PEIGel (dose equivalent to 100 μg α-PDL1) was injected into the tumor bed. After 30 days of therapy, the tumors were collected for histological and flow cytometric analyses. b Photographs of resected recurrent tumors from mice treated with PBS, PEIGel, α-PDL1 or α-PDL1/PEIGel (intratumoral injection, dose equivalent to 100 μg α-PDL1). c Average tumor weights of recurrent tumors in 4T1-bearing mice treated with PBS, PEIGel, α-PDL1 or α-PDL1/PEIGel ($n = 6$). d Average tumor volumes of metastatic tumors in 4T1 tumor-bearing mice treated with PBS, PEIGel, α-PDL1 or α-PD-L1/PEIGel (intratumoral injection, dose equivalent to 100 μg anti-PDL1, $n = 6$). e Individual tumor volumes of recurrent tumors in mice treated with PBS, the PEIGel, α-PDL1 or the α-PDL1/PEIGel (intratumoral injection, dose equivalent to 100 μg anti-PDL1), n = 6 biologically independent mice per group. f, h Flow cytometric analysis and g, i quantitative analysis of $CD8^+$ T cells after gating on $CD45^+CD3^+$ cells and IFN-γ^+ T cells after gating on $CD45^+CD3^+CD8^+$ cells, n = 3 biologically independent mice per group. Data are shown as the mean ± SD; statistical analysis was performed by one-way ANOVA with Tukey's post-hoc test. $^*P < 0.05$, $^{**}P < 0.01$, $^{***}P < 0.001$, $^{****}P < 0.0001$.

clearance (CCr) did not change greatly, suggesting that α-PDL1/PEIGel had low toxicity to the liver and kidneys. By subcutaneous injection of PEIGel, its degradation process in vivo can be observed, and the content can be reduced by about 90% at 25 days (Supplementary Fig. 17). In addition, H&E staining (Supplementary Fig. 18) did not detect obvious pathological variations in the major organs, including the heart, liver, spleen, lungs and kidneys, further proving the good biosafety of the α-PDL1/PEIGel. These data, together with data showing stable weights and temperatures for mice (Supplementary Figs. 19 and 20) during treatment, indicated that the α-PDL1/PEIGel showed satisfactory biocompatibility, suggesting that the PEIGel holds great potential to be translated into a clinical treatment for solid tumors.

3. Discussion

Local administration of ICB therapeutics has been demonstrated to be an effective strategy for enhancing efficacy and safety, as this approach can mitigate the adverse effects of nonspecific systemic distribution and increase in situ bioavailability [5]. Moreover, if immunomodulators are formulated in a synthetic hydrogel, their release kinetics and pharmacodynamics can be drastically improved and precisely controlled. As a result of extending local release, systemic immunotherapeutic effects can be significantly enhanced, resulting in suppression of primary and metastatic malignancies and even prevention of tumor recurrence after surgical resection [56].

With the rapid growth of research on hydrogel-based immunomodulator delivery, interest in developing immunotherapeutic hydrogels with innate immune modulation functions is expanding. In this study, we designed a PEIGel with α-PDL1 embedded to combat murine breast tumors in a mouse model. Our results showed that PEIGel could reshape the immunosuppressive TME by upregulating PDL1 expression and promoting M1-like macrophage polarization, thus synergizing with α-PDL1 to eliminate both primary tumors and metastatic tumors. This modulatory effect of PEIGel can be partly due to the intrinsic immune adjuvant effects of PEI [39]. Interestingly, a preliminary mechanistic study implied a potential correlation between PEI's immune adjuvanticity and its polyamine metabolism/catabolism modulation ability. This study not only helps us design next-generation scaffold hydrogels for extended release but also deepens our understanding of the physiological function of PEI.

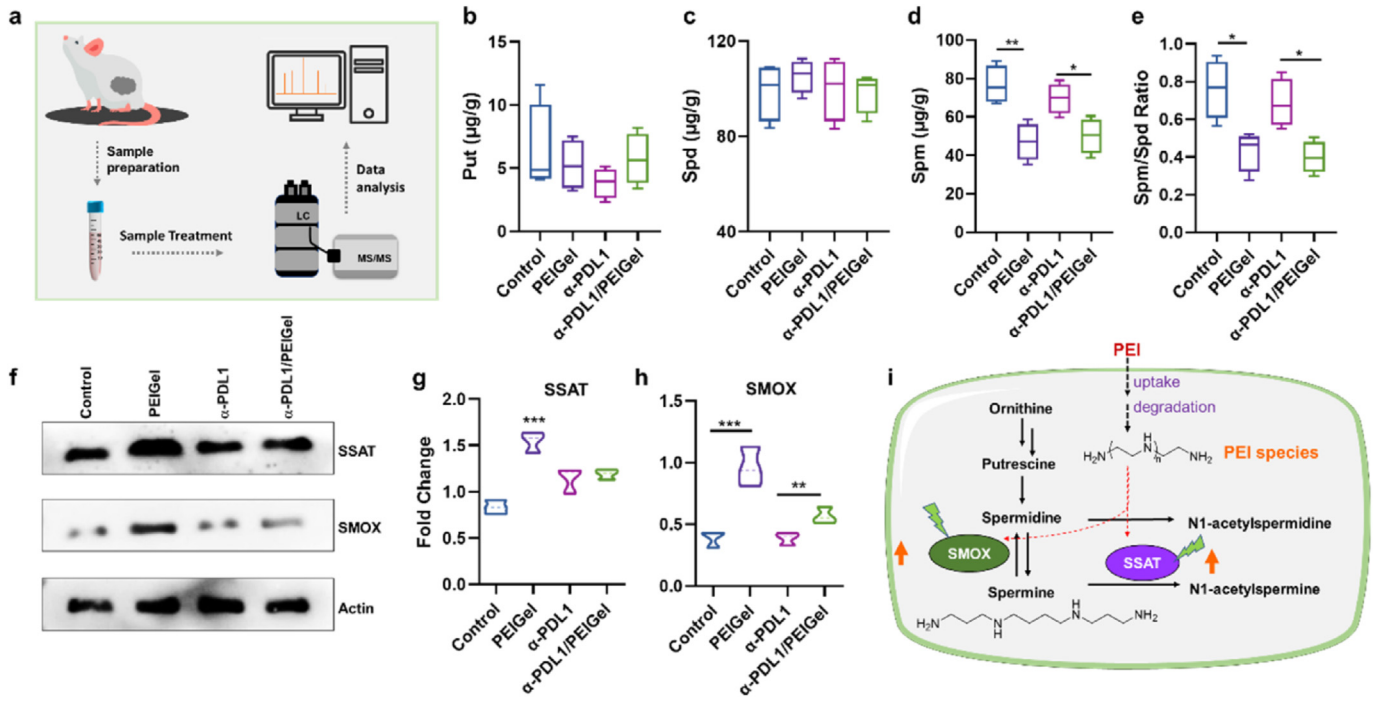

Fig. 7. PEIGel modulates the intratumoral polyamine levels and acts as an inducer of SSAT. a Schematic of the procedures for polyamine quantification in 4T1 tumors using the UPLC-mass method. 4T1 tumor-bearing mice were intratumorally injected with 100 μL PBS, PEIGel, α-PDL1, or α-PDL1/PEIGel (dose equivalent to 100 μg α-PDL1) on day 0, and tumor samples were collected on day 14 for polyamine detection. b-d Intratumoral putrescine (put), spermidine (spd), and spermine (spm) levels. $n = 4$ biologically independent mice per group. e Spermine to spermidine ratio (spm:spd). f Western blot analysis of SSAT and SMOX associated with polyamine catabolism in 4T1 tumors following two weeks of treatment. g, h SSAT and SMOX expression fold change against β-actin. i Proposed mechanism for polyamine catabolism modulation induced by PEI. Data are presented as the mean ± SD. Statistical analysis was performed by one-way ANOVA with Tukey's post-hoc test. $^{*}P < 0.05$, $^{**}P < 0.01$, $^{***}P < 0.001$, $^{****}P < 0.0001$.

In summary, our results suggested that the PEIGel encapsulating α-PDL1 is a superb "drug-in-adjuvant" formulation for treating immunologically "cold" murine breast tumors. Unlike most traditional "scaffold hydrogels", our PEIGel defined a new paradigm of immunotherapeutic hydrogels, which not only function as carriers for immunomodulators but also directly engage in modulating the TME. These dual functions could harmonize in the tumor milieu to potentiate immunotherapeutic efficacy *via* several mechanisms. Overall, it is reasonable to conclude that PEIGel might be a versatile platform for the local delivery of different kinds of immunomodulators for immune adjuvant-synergized cancer immunotherapy.

4. Methods

4.1. Materials

PEI (Catalog No. E107077, M.W. ~600) and PVA (Catalog No. P105126, M.W. 89000–98000) were purchased from Aladdin (Shanghai, China). Magnesium chloride (MgCl2, Catalog No. A60905) was obtained from 3AChem (Shanghai, China). α-PDL1 (Catalog No. BE0101) was obtained from BioXCell (New Hampshire, USA). AF647-α-PDL1 (Catalog No. E-AB-F1132UM) was purchased from Elabscience (Wuhan, China). A Masson staining kit (Catalog No. G1006), a TUNEL assay kit (Servicebio, Catalog No. G1501), DAPI (Catalog No. G1012) and antibodies specific for PDL1 (Catalog No. GB11339), CD3 (Catalog No. GB111337), CD8 (Catalog No. GB11068), and Ki67 (Catalog No. GB111499) were obtained from Servicebio (Wuhan, China). Antibodies for flow cytometric analysis specific for CD45 (Catalog No. 103116), CD3 (Catalog No. 100306), CD8 (Catalog No. 100722), CD4 (Catalog No. 100559), FOXP3 (Catalog No. 17-5773-82), IFN-γ (Catalog No. 505830), CD11B (Catalog No. 101251), F4/80 (Catalog No. 123122), MHC II (Catalog No. 107606), CD11c (Catalog No. 117310), CD80 (Catalog No. 104708), CD86 (Catalog No. 105040), and CD206 (Catalog No. 141720) were purchased from BioLegend (California, USA). IL-2 (Catalog No. MU30009), IL-6 (Catalog No. MU30044), TNF-α (Catalog No. MU30030), and IFN-γ (Catalog No. MU30038) ELISA kits were purchased from Bioswamp (Wuhan, China).

4.2. Cell lines

Cells, including 4T1 cells (murine breast cancer cells),AML-12 cells (murine normal liver cells), HUVECs cells (human umbilical vein endothelial cells) were purchased from American Type Culture Collection (Manassas, VA). All cells were cultured in RPMI-1640 supplemented with 10% fetal bovine serum, 100 units/mL penicillin and 50 units/mL streptomycin at 37 °C in a humidified incubator with a 5% CO_2 atmosphere.

4.3. Animals

All animals used in this study were purchased from SPF Biotechnology Inc. (Beijing, China). All animal experiments were performed in accordance with the protocols of the Jinan University Animal Ethics Board. 4T1 cell xenograft mouse models were established by subcutaneous (*s.c.*) injection of 1×10^6 4T1 cells into Balb/C mice and monitored until the tumor volume reached 100–130 mm^3.

4.4. Preparation and characterization of the PVA-PEI hydrogel

First, 1 g PEI and 12 mg Mg^{2+} were weighed and dissolved in 9 mL deionized water. Then, 2 g PVA was added to the above solution with stirring at 10 rpm and 98 °C until a uniform PEIGel was obtained. Then, the as-prepared PEIGel was cooled to 37 °C and added to 8.29 mg/mL α-PDL1 at a volume ratio of 100:12. After homogeneous mixing, the

α-PDL1/PEIGel was finally obtained for subsequent *in vitro* or in vivo experiments.

The morphology and physiochemical properties of the as-prepared α-PDL1/PEIGel were investigated by cryo-SEM (HITACHI, SU 8020, Japan), FT-IR (Bruker, VERTEX80v, USA) and DMA (TA Instruments, Q800, USA).

4.5. In vitro release profile of the PVA-PEI hydrogel

The *in vitro* release profile of α-PDL1 was evaluated as previously described. In brief, 2 mL α-PDL1/PEIGel was immersed in 10 mL 1 × PBS buffer at room temperature for 4 weeks, during which time samples were collected at the time points 1, 3, 6, 12, 36, 72, 168, 336 and 672 h. Then, the content of α-PDL1 in the collected samples was determined with a UV–Vis spectrophotometer (Shimadzu, UV-3600, Japan).

4.6. In vivo release profile of the PVA-PEI hydrogel

To further elucidate the release profile of the PEIGel in vivo, mice bearing 4T1 cell xenografts were randomly divided into two groups for fluorescence imaging with an IVIS spectrum system (PerkinElmer, Lumina III, USA). The mice in the control group were intratumorally injected with free α-PDL1 solution (1 mg/mL, 100 μL), and those in the α-PDL1/PEIGel group were intratumorally injected with the α-PDL1/PEIGel (dose equivalent to 100 μg a-PDL1). Fluorescence images were then captured at specific time points (days 1, 3, 7, 14, 21, and 28). The fluorescence intensity at the time points was quantified by Living Image software (PerkinElmer, v4.4, Massachusetts, USA).

4.7. Antitumor efficacy of the PVA-PEI hydrogel in a xenograft tumor model

To evaluate antitumor efficacy in vivo, 4T1 cell xenograft mouse models were used to assess the inhibitory effect of the α-PDL1/PEIGel on 4T1 tumor growth. Briefly, mice bearing 4T1 cell xenografts were divided into 4 groups: (1) control group: intratumoral injection of 100 μL saline solution; (2) PEIGel group: intratumoral injection of 100 μL PEIGel (120 μg Mg^{2+}); (3) α-PDL1 group: intratumoral injection of 100 μL α-PDL1 solution (1 mg/mL, dose: 100 μg α-PDL1); and (4) α-PDL1/PEIGel group: intratumoral injection of 100 μL α-PDL1/PEIGel (dose equivalent to 100 μg α-PDL1, 120 μg Mg^{2+}). The different treatments were administered on day 0. Mouse weight, temperature and tumor volume were recorded every 4 days. Blood samples were collected on days 7, 14 and 21 for the detection of serum IL-2, IL-6, TNF-α and IFN-γ levels with corresponding ELISA kits according to the protocols provided by the manufacturers. Kaplan–Meier survival analysis was performed using an endpoint tumor volume of 1000 mm^3 as a surrogate for mortality. The log-rank test was used for comparisons of survival among the different groups.

4.8. Antitumor efficacy of the PVA-PEI hydrogel in a metastatic tumor model

To further evaluate the antitumor efficacy of the α-PDL1/PEIGel in a metastatic tumor model, 1 × 10^6 4T1 cells were *s.c.* injected into the left hindlimb of Balb/C mice and allowed to grow until the tumor volume reached 100–130 mm^3. Then, the mice were divided into 4 groups: (1) control group: intratumoral injection of 100 μL saline solution; (2) PEIGel group: intratumoral injection of 100 μL PEIGel(120 μg Mg^{2+}); (3) α-PDL1 group: intratumoral injection of 100 μL α-PDL1 solution (1 mg/mL, dose: 100 μg α-PDL1); and (4) α-PDL1/PEIGel group: intratumoral injection of 100 μL α-PDL1/PEIGel (dose equivalent to 100 μg α-PDL1, 120 μg Mg^{2+}). Meanwhile, the right hindlimb was also *s.c.* injected with 1 × 10^6 4T1 cells to establish a metastatic tumor model, followed by intratumoral injection of the different treatments (day 0). Mouse weight, temperature and tumor volume were recorded every 2 days. The whole treatment period lasted 16 days. After that, the tumors in the right hindlimb from the different treatment groups were collected for flow cytometric analysis, ELISA and immunofluorescence analysis.

4.9. Antitumor efficacy of the PVA-PEI hydrogel in a recurrent tumor model

The antitumor efficacy of the α-PDL1/PEIGel in a recurrent tumor model was also investigated. In brief, 1 × 10^6 4T1 cells were *s.c.* injected into the left hindlimb of Balb/C mice and allowed to grow until the tumor volume reached 100–130 mm^3. Then, the mice were anesthetized, the tumor was partially resected, leaving a tumor recurrence bed. After that, the recurrent tumor model mice were divided into 4 groups: (1) control group: intratumoral injection of 100 μL saline solution; (2) PEIGel group: intratumoral injection of 100 μL PEIGel(120 μg Mg^{2+}); (3) α-PDL1 group: intratumoral injection of 100 μL α-PDL1 solution (1.0 mg/mL, dose: 100 μg α-PDL1); and (4) α-PDL1/PEIGel group: intratumoral injection of 100 μL α-PDL1/PEIGel (dose equivalent to 100 μg α-PDL1, 120 μg Mg^{2+}). The different treatments were administered on day 0. Mouse weight, temperature and tumor volume were recorded every 3 days. The whole treatment period lasted 30 days. After that, all mice were euthanized, and the tumors from the different treatment groups were collected for flow cytometric analysis.

4.10. Polyamine level determination

Fifty milligrams of the sample was accurately weighed into a centrifuge tube, and 0.5 mL of 0.1 M hydrochloric acid, vortexed, and extracted for 1 h at room temperature. The samples were centrifuged at 12000 rpm for 10 min, and the supernatant was collected. A 10 μL sample was placed into a bottle, and 70 μL of AccQ•Tag Ultra Borate buffer and 20 μL of AccQ•Tag reagent were added. The reaction mixture was heated at 55 °C for 10 min and then tested on a computer after cooling. The sample extracts were analyzed using a UPLC–Orbitrap-MS system (UPLC, Vanquish; MS, QE). HRMS data were recorded on a Q Exactive hybrid Q–Orbitrap mass spectrometer equipped with a heated ESI source (Thermo Fisher Scientific) utilizing the SIM MS acquisition methods. Data were acquired on the Q-Exactive using Xcalibur 4.1 (Thermo Scientific) and processed using TraceFinder™4.1 Clinical (Thermo Scientific).

4.11. Western blot

RIPA lysis solution (containing protease inhibitor) was added to the tumor tissue sample, ground or lysed on ice, ultrasonically homogenized, and centrifuged, and the supernatant was collected. After the total protein extraction of the sample was completed, the protein stock solution was serially diluted, and the protein concentration was detected by the BCA method. An appropriate amount of protein was used for electrophoresis. The western blot was transferred to a nitrocellulose membrane with a membrane transfer device and blocked for 1 h. The primary antibody was added, and the membrane was blocked overnight (SSAT, SMOX, PD-L1, CD86,Abcam, USA), rinsed with PBS, added dropwise to the secondary antibody, and incubated for 1 h at room temperature. The membranes were developed by chemiluminescence, and the results were analyzed by ImageJ image analysis software.

4.12. Flow cytometric analysis

Collected tumors from different treatment groups were cut into ~ 1- to 2-mm^3 pieces, placed on a 200-mesh sieve, and thoroughly ground with a 1-mL syringe, during which PBS was used to rinse the tissues and collect cells. The cells were then obtained by filtration through a 40-μm filter, followed by centrifugation at 1500 rpm for 7 min. After that, the cells were dispersed in a 35% Percoll solution, and tumor-infiltrating lymphocytes (TILs) were obtained by centrifugation at 600×*g* for 15

min. The TILs were stained with anti-CD45-APC-Cy7, anti-CD3-FITC, anti-CD8-PE-Cy7, anti-CD4-BV510, anti-Foxp3-APC, anti–IFN–γ-BV421, or anti-CD45-APC-Cy7, anti-CD11B-BV421, anti-F4/80-APC, anti-CD11C-PerCP-Cy5.5, anti-CD80-PE, anti-CD86-BV510, anti-CD206-PE-Cy7, and anti-MHC–II–FITC for flow cytometric analysis (BD, FACS-Verse, USA). Cell subsets were analyzed with FlowJo 10.7.1 software as described in a previous study.

4.13. Immunofluorescence analysis

Briefly, tumor sections from different treatment groups were dewaxed and then immersed in PBST. Antigen retrieval was performed with heating in a microwave oven for 45 s. After cooling, the tumor sections were covered with 3% hydrogen peroxide for 5 min to inactivate endogenous peroxidases and then washed in PBST 3 times. Then, the tumor sections were blocked with 10% BSA for 30 min and incubated with corresponding fluorophore-labeled antibodies (antibodies specific for Ki-67, CD3, CD8, and PD-L1 and TUNEL staining reagents) overnight at 4 °C. The slides were finally washed with PBST three times and mounted for further observation. The microscopic data were analyzed by using ImageJ software (National Institutes of Health, v1.47, USA).

4.14. Hematoxylin and eosin staining

Major organs, including the tumor, heart, liver, spleen, lungs and kidneys, were collected and fixed with 4% paraformaldehyde. The tissues were then sliced by the paraffin sectioning method and dried. The sections were then rehydrated in water, followed by hematoxylin staining for 2 min and eosin staining for 40 s. The stained sections were finally mounted with permanent mounting medium for further evaluation by optical microscopy.

4.15. Toxicity of the PVA-PEI hydrogel

To evaluate the biocompatibility of the α-PDL1/PEIGel, 16 Balb/C mice were divided into 4 groups. The mice in each group were subcutaneously administered 100 μL PBS, PEIGel, α-PDL1 or α-PDL1/PEIGel and fed for 30 days. Body temperature and weight were monitored every 3 days. After that, serum was obtained from collected blood samples *via* centrifugation at 3000 rpm. The levels of blood parameters, including WBCs, RBCs, PLTs, HGB, ALB, GLB, ALT, AST, LDH, urea, Cys C and CCr, in the serum were determined with an automatic biochemical analyzer (Rayto, Chemray420, Shenzhen, China). Tissue sections (heart, liver, spleen, lung and kidney) stained with H&E were observed by optical microscopy to detect pathological changes in the tissues.

4.16. Statistical analysis

All values are expressed as the mean ± SD. Intergroup comparisons were made using a two-tailed Student's *t*-test or one-way ANOVA by GraphPad Prism for Windows (GraphPad Software Inc., version 8.0, USA), and $*P < 0.05$ was considered statistically significant.

Author contributions

L.L., K.H., M.Z. and Z.L. conceived and planned the experiments. Y.Y. and C.W. conducted the experiments related to the synthesis and characterization of the hydrogel. Z.X., Z.C., D.W., C.H., L.X., L.L.Z., L.L.X. and K.H. performed the experiments and analyzed the data for the *in vitro* and in vivo studies. K.H., Z.X. and D.W. wrote the manuscript, which was reviewed and edited by all coauthors.

Data availability

All relevant data are available from the authors.

Declaration of competing interest

The authors declare that they have no known competing financial interests or personal relationships that could have appeared to influence the work reported in this paper.

Acknowledgments

This work was supported by the Natural Science Foundation of China (Grant Nos. 81771973, 81971672, 21801019, and 61875015), the Guangzhou Key Laboratory of Molecular and Functional Imaging for Clinical Translation (201905010003), the China Postdoctoral Science Foundation (2019M663392), the Beijing Natural Science Foundation (JQ20038), the AMED Moonshot Research and Development Program (Grant No 21zf0127003h001), JSPS KAKENHI (Grant Nos. 21H02873 and 20H03635), and the JSPS International Joint Research Program (JPJSBP120207203).

Appendix A. Supplementary data

Supplementary data to this article can be found online at https://doi.org/10.1016/j.mtbio.2022.100297.

References

[1] J. Li, D.J. Mooney, Designing hydrogels for controlled drug delivery, Nat. Rev. Mater. 1 (12) (2016) 1–17.
[2] X. Han, H. Li, D. Zhou, Z. Chen, Z. Gu, Local and targeted delivery of immune checkpoint blockade therapeutics, Acc. Chem. Res. 53 (11) (2020) 2521–2533.
[3] B. Pelaz, C. Alexiou, R.A. Alvarez-Puebla, F. Alves, A.M. Andrews, S. Ashraf, L.P. Balogh, L. Ballerini, A. Bestetti, C. Brendel, S. Bosi, M. Carril, W.C.W. Chan, C. Chen, X. Chen, X. Chen, Z. Cheng, D. Cui, J. Du, C. Dullin, A. Escudero, N. Feliu, M. Gao, M. George, Y. Gogotsi, A. Grünweller, Z. Gu, N.J. Halas, N. Hampp, R.K. Hartmann, M.C. Hersam, P. Hunziker, J. Jian, X. Jiang, P. Jungebluth, P. Kadhiresan, K. Kataoka, A. Khademhosseini, J. Kopeček, N.A. Kotov, H.F. Krug, D.S. Lee, C.-M. Lehr, K.W. Leong, X.-J. Liang, M. Ling Lim, L.M. Liz-Marzán, X. Ma, P. Macchiarini, H. Meng, H. Möhwald, P. Mulvaney, A.E. Nel, S. Nie, P. Nordlander, T. Okano, J. Oliveira, T.H. Park, R.M. Penner, M. Prato, V. Puntes, V.M. Rotello, A. Samarakoon, R.E. Schaak, Y. Shen, S. Sjöqvist, A.G. Skirtach, M.G. Soliman, M.M. Stevens, H.-W. Sung, B.Z. Tang, R. Tietze, B.N. Udugama, J.S. VanEpps, T. Weil, P.S. Weiss, I. Willner, Y. Wu, L. Yang, Z. Yue, Q. Zhang, Q. Zhang, X.-E. Zhang, Y. Zhao, X. Zhou, W.J. Parak, Diverse applications of nanomedicine, ACS Nano 11 (3) (2017) 2313–2381.
[4] M. Sepantafar, R. Maheronnaghsh, H. Mohammadi, F. Radmanesh, M.M. Hasani-Sadrabadi, M. Ebrahimi, H. Baharvand, Engineered hydrogels in cancer therapy and diagnosis, Trends Biotechnol. 35 (11) (2017) 1074–1087.
[5] I. Melero, E. Castanon, M. Alvarez, S. Champiat, A. Marabelle, Intratumoural administration and tumour tissue targeting of cancer immunotherapies, Nat. Rev. Clin. Oncol. (2021) 1–19.
[6] W.X. Hong, S. Haebe, A.S. Lee, C.B. Westphalen, J.A. Norton, W. Jiang, R. Levy, Intratumoral immunotherapy for early-stage solid tumors, Clin. Cancer Res. 26 (13) (2020) 3091–3099.
[7] S. Correa, A.K. Grosskopf, H. Lopez Hernandez, D. Chan, A.C. Yu, L.M. Stapleton, E.A. Appel, Translational Applications of hydrogels, Chem. Rev., 2021.
[8] F. Wang, D. Xu, H. Su, W. Zhang, X. Sun, M.K. Monroe, R.W. Chakroun, Z. Wang, W. Dai, R. Oh, Supramolecular prodrug hydrogelator as an immune booster for checkpoint blocker–based immunotherapy, Sci. Adv. 6 (18) (2020), eaaz8985.
[9] C. Song, H. Phuengkham, Y.S. Kim, I. Lee, I.W. Shin, H.S. Shin, S.M. Jin, S.H. Um, H. Lee, K.S. Hong, Syringeable immunotherapeutic nanogel reshapes tumor microenvironment and prevents tumor metastasis and recurrence, Nat. Commun. 10 (1) (2019) 1–15.
[10] C.G. Park, C.A. Hartl, D. Schmid, E.M. Carmona, H.J. Kim, M.S. Goldberg, Extended release of perioperative immunotherapy prevents tumor recurrence and eliminates metastases, Sci. Transl. Med. 10 (433) (2018) eaar1916.
[11] F. Wang, H. Su, D. Xu, W. Dai, W. Zhang, Z. Wang, C.F. Anderson, M. Zheng, R. Oh, F. Wan, Tumour sensitization via the extended intratumoural release of a STING agonist and camptothecin from a self-assembled hydrogel, Nat. Biomed. Eng. 4 (11) (2020) 1090–1101.

[12] Q. Hu, H. Li, E. Archibong, Q. Chen, H. Ruan, S. Ahn, E. Dukhovlinova, Y. Kang, D. Wen, G. Dotti, Inhibition of post-surgery tumour recurrence via a hydrogel releasing CAR-T cells and anti-PDL1-conjugated platelets, Nat. Biomed. Eng. (2021) 1–10.
[13] P. Zhang, Y. Zhai, Y. Cai, Y. Zhao, Y. Li, Nanomedicine-based immunotherapy for the treatment of cancer metastasis, Adv. Mater. 31 (49) (2019) 1904156.
[14] L. Galluzzi, A. Buqué, O. Kepp, L. Zitvogel, G. Kroemer, Immunogenic cell death in cancer and infectious disease, Nat. Rev. Immunol. 17 (2) (2017) 97–111.
[15] K.J. Hiam-Galvez, B.M. Allen, M.H. Spitzer, Systemic immunity in cancer, Nat. Rev. Cancer 21 (6) (2021) 345–359.
[16] L. Li, J. Zou, Y. Dai, W. Fan, G. Niu, Z. Yang, X. Chen, Burst release of encapsulated annexin A5 in tumours boosts cytotoxic T-cell responses by blocking the phagocytosis of apoptotic cells, Nat. Biomed. Eng. 4 (11) (2020) 1102–1116.
[17] L. Li, Y. Li, C.H. Yang, D.C. Radford, J. Wang, M. Janát-Amsbury, J. Kopeček, J. Yang, Inhibition of immunosuppressive tumors by polymer-assisted inductions of immunogenic cell death and multivalent PD-L1 crosslinking, Adv. Funct. Mater. 30 (12) (2020), 1908961.
[18] M.A. Postow, R. Sidlow, M.D. Hellmann, Immune-related adverse events associated with immune checkpoint blockade, N. Engl. J. Med. 378 (2) (2018) 158–168.
[19] J. Michot, C. Bigenwald, S. Champiat, M. Collins, F. Carbonnel, S. Postel-Vinay, A. Berdelou, A. Varga, R. Bahleda, A. Hollebecque, Immune-related adverse events with immune checkpoint blockade: a comprehensive review, Eur. J. Cancer 54 (2016) 139–148.
[20] C. Dolladille, S. Ederhy, M. Sassier, J. Cautela, F. Thuny, A.A. Cohen, S. Fedrizzi, B. Chrétien, A. Da-Silva, A.-F. Plane, Immune checkpoint inhibitor rechallenge after immune-related adverse events in patients with cancer, JAMA Oncol. 6 (6) (2020) 865–871.
[21] F.R. Balkwill, M. Capasso, T. Hagemann, The tumor microenvironment at a glance, J. Cell Sci. 125 (23) (2012) 5591–5596.
[22] M. de Miguel, E. Calvo, Clinical challenges of immune checkpoint inhibitors, Cancer Cell 38 (3) (2020) 326–333.
[23] Z. Li, Y. Wang, Y. Shen, C. Qian, D. Oupicky, M. Sun, Targeting pulmonary tumor microenvironment with CXCR4-inhibiting nanocomplex to enhance anti–PD-L1 immunotherapy, Sci. Adv. 6 (20) (2020) eaaz9240.
[24] C. Wang, J. Wang, X. Zhang, S. Yu, D. Wen, Q. Hu, Y. Ye, H. Bomba, X. Hu, Z. Liu, In situ formed reactive oxygen species–responsive scaffold with gemcitabine and checkpoint inhibitor for combination therapy, Sci. Transl. Med. 10 (429) (2018), eaan3682.
[25] H. Wang, A.J. Najibi, M.C. Sobral, B.R. Seo, J.Y. Lee, D. Wu, A.W. Li, C.S. Verbeke, D.J. Mooney, Biomaterial-based scaffold for in situ chemo-immunotherapy to treat poorly immunogenic tumors, Nat. Commun. 11 (1) (2020) 1–14.
[26] Y. Chao, L. Xu, C. Liang, L. Feng, J. Xu, Z. Dong, L. Tian, X. Yi, K. Yang, Z. Liu, Combined local immunostimulatory radioisotope therapy and systemic immune checkpoint blockade imparts potent antitumour responses, Nat. Biomed. Eng. 2 (8) (2018) 611–621.
[27] J. Zhang, C. Chen, A. Li, W. Jing, P. Sun, X. Huang, Y. Liu, S. Zhang, W. Du, R. Zhang, Y. Liu, A. Gong, J. Wu, X. Jiang, Immunostimulant hydrogel for the inhibition of malignant glioma relapse post-resection, Nat. Nanotechnol. 16 (2021) 538–548.
[28] Q. Chen, C. Wang, X. Zhang, G. Chen, Q. Hu, H. Li, J. Wang, D. Wen, Y. Zhang, Y. Lu, G. Yang, C. Jiang, J. Wang, G. Dotti, Z. Gu, In situ sprayed bioresponsive immunotherapeutic gel for post-surgical cancer treatment, Nat. Nanotechnol. 14 (1) (2019) 89–97.
[29] L. Huang, Y. Li, Y. Du, Y. Zhang, X. Wang, Y. Ding, X. Yang, F. Meng, J. Tu, L. Luo, C. Sun, Mild photothermal therapy potentiates anti-PD-L1 treatment for immunologically cold tumors via an all-in-one and all-in-control strategy, Nat. Commun. 10 (1) (2019) 4871.
[30] X. Dong, R. Cheng, S. Zhu, H. Liu, R. Zhou, C. Zhang, K. Chen, L. Mei, C. Wang, C. Su, X. Liu, Z. Gu, Y. Zhao, A heterojunction structured WO2.9-WSe2 nanoradiosensitizer increases local tumor ablation and checkpoint blockade immunotherapy upon low radiation dose, ACS Nano 14 (5) (2020) 5400–5416.
[31] J. Wang, Y. Li, G. Nie, Multifunctional biomolecule nanostructures for cancer therapy, Nat. Rev. Mater. 6 (9) (2021) 766–783.
[32] Y. Shao, B. Liu, Z. Di, G. Zhang, L.-D. Sun, L. Li, C.-H. Yan, Engineering of upconverted metal–organic frameworks for near-infrared light-triggered combinational photodynamic/chemo-/immunotherapy against hypoxic tumors, J. Am. Chem. Soc. 142 (8) (2020) 3939–3946.
[33] M. Cao, R. Cai, L. Zhao, M. Guo, L. Wang, Y. Wang, L. Zhang, X. Wang, H. Yao, C. Xie, Y. Cong, Y. Guan, X. Tao, Y. Wang, S. Xu, Y. Liu, Y. Zhao, C. Chen, Molybdenum derived from nanomaterials incorporates into molybdenum enzymes and affects their activities in vivo, Nat. Nanotechnol. 16 (6) (2021) 708–716.
[34] W. Huang, L. He, J. Ouyang, Q. Chen, C. Liu, W. Tao, T. Chen, Triangle-shaped tellurium nanostars potentiate radiotherapy by boosting checkpoint blockade immunotherapy, Matter 3 (5) (2020) 1725–1753.
[35] D. Wang, J. Zhou, W. Fang, C. Huang, Z. Chen, M. Fan, M.R. Zhang, Z. Xiao, K. Hu, L. Luo, A multifunctional nanotheranostic agent potentiates erlotinib to EGFR wild-type non-small cell lung cancer, Bioact. Mater. 13 (2022) 312–323.
[36] A. Kichler, C. Leborgne, E. Coeytaux, O. Danos, Polyethylenimine-mediated gene delivery: a mechanistic study, J. Gene Med. 3 (2) (2001) 135–144.
[37] C. Shen, J. Li, Y. Zhang, Y. Li, G. Shen, J. Zhu, J. Tao, Polyethylenimine-based micro/nanoparticles as vaccine adjuvants, Int. J. Nanomed. 12 (2017) 5443–5460.
[38] K. Regnström, E.G.E. Ragnarsson, M. Köping-Höggård, E. Torstensson, H. Nyblom, P. Artursson, Pei – a potent, but not harmless, mucosal immuno-stimulator of mixed T-helper cell response and FasL-mediated cell death in mice, Gene Ther. 10 (18) (2003) 1575–1583.
[39] F. Wegmann, K.H. Gartlan, A.M. Harandi, S.A. Brinckmann, M. Coccia, W.R. Hillson, W.L. Kok, S. Cole, L.-P. Ho, T. Lambe, M. Puthia, C. Svanborg, E.M. Scherer, G. Krashias, A. Williams, J.N. Blattman, P.D. Greenberg, R.A. Flavell, A.E. Moghaddam, N.C. Sheppard, Q.J. Sattentau, Polyethyleneimine is a potent mucosal adjuvant for viral glycoprotein antigens, Nat. Biotechnol. 30 (9) (2012) 883–888.
[40] C. Wang, K. Hu, C. Zhao, Y. Zou, Y. Liu, X. Qu, D. Jiang, Z. Li, M.R. Zhang, Z. Li, Customization of conductive elastomer based on PVA/PEI for stretchable sensors, Small 16 (7) (2020) 1904758.
[41] C. Wang, Z. Di, Z. Xiang, J. Zhao, L. Li, Coordination-driven assembly of proteins and nucleic acids in a single architecture for carrier-free intracellular co-delivery, Nano Today 38 (2021) 101140.
[42] J. Lötscher, A.-A. Martí i Líndez, N. Kirchhammer, E. Cribioli, G.M.P. Giordano Attianese, M.P. Trefny, M. Lenz, S.I. Rothschild, P. Strati, M. Künzli, C. Lotter, S.H. Schenk, P. Dehio, J. Löliger, L. Litzler, D. Schreiner, V. Koch, N. Page, D. Lee, J. Grählert, D. Kuzmin, A.-V. Burgener, D. Merkler, M. Pless, M.L. Balmer, W. Reith, J. Huwyler, M. Irving, C.G. King, A. Zippelius, C. Hess, Magnesium sensing via LFA-1 regulates CD8+ T cell effector function, Cell 185 (4) (2022) 585–602, e29.
[43] D.B. Doroshow, S. Bhalla, M.B. Beasley, L.M. Sholl, K.M. Kerr, S. Gnjatic, Wistuba II, D.L. Rimm, M.S. Tsao, F.R. Hirsch, PD-L1 as a biomarker of response to immune-checkpoint inhibitors, Nat. Rev. Clin. Oncol. 18 (6) (2021) 345–362.
[44] M. Guo, X. Zhang, J. Liu, F. Gao, X. Zhang, X. Hu, B. Li, X. Zhang, H. Zhou, R. Bai, Y. Wang, J. Li, Y. Liu, Z. Gu, C. Chen, Few-layer Bismuthene for checkpoint knockdown enhanced cancer immunotherapy with rapid clearance and sequentially triggered one-for-all strategy, ACS Nano 14 (11) (2020) 15700–15713.
[45] D.J. Puleston, F. Baixauli, D.E. Sanin, J. Edwards-Hicks, M. Villa, A.M. Kabat, M.M. Kamiński, M. Stanckzak, H.J. Weiss, K.M. Grzes, Polyamine metabolism is a central determinant of helper T cell lineage fidelity, Cell, 2021. S0092–8674(21) 00708–X.
[46] A. Wagner, C. Wang, J. Fessler, D. DeTomaso, J. Avila-Pacheco, J. Kaminski, S. Zaghouani, E. Christian, P. Thakore, B. Schellhaass, Metabolic modeling of single Th17 cells reveals regulators of Autoimmunity, Cell, 2021.
[47] R.A. Casero Jr., T. Murray Stewart, A.E. Pegg, Polyamine metabolism and cancer: treatments, challenges and opportunities, Nat. Rev. Cancer 18 (11) (2018) 681–695.
[48] I. Roci, J.D. Watrous, K.A. Lagerborg, L. Lafranchi, A. Lindqvist, M. Jain, R. Nilsson, Mapping metabolic events in the cancer cell cycle reveals arginine catabolism in the committed SG2M phase, Cell Rep. 26 (7) (2019) 1691–1700, e5.
[49] R. Wu, X. Chen, S. Kang, T. Wang, J.R. Gnanaprakasam, Y. Yao, L. Liu, G. Fan, M.R. Burns, R. Wang, De novo synthesis and salvage pathway coordinately regulate polyamine homeostasis and determine T cell proliferation and function, Sci. Adv. 6 (51) (2020), eabc4275.
[50] G.M. Carriche, L. Almeida, P. Stüve, L. Velasquez, A. Dhillon-LaBrooy, U. Roy, M. Lindenberg, T. Strowig, C. Plaza-Sirvent, I. Schmitz, Regulating T-cell differentiation through the polyamine spermidine, J. Allergy Clin. Immunol. 147 (1) (2021) 335–348, e11.
[51] V. Bronte, P. Zanovello, Regulation of immune responses by L-arginine metabolism, Nat. Rev. Immunol. 5 (8) (2005) 641–654.
[52] R.A. Casero, L.J. Marton, Targeting polyamine metabolism and function in cancer and other hyperproliferative diseases, Nat. Rev. Drug Discov. 6 (5) (2007) 373–390.
[53] H.C. Affronti, A.M. Rowsam, A.J. Pellerite, S.R. Rosario, M.D. Long, J.J. Jacobi, A. Bianchi-Smiraglia, C.S. Boerlin, B.M. Gillard, E. Karasik, B.A. Foster, M. Moser, J.H. Wilton, K. Attwood, M.A. Nikiforov, G. Azabdaftari, R. Pili, J.G. Phillips, R.A. Casero Jr., D.J. Smiraglia, Pharmacological polyamine catabolism upregulation with methionine salvage pathway inhibition as an effective prostate cancer therapy, Nat. Commun. 11 (1) (2020) 52.
[54] A. Khan, L.D. Gamble, D.H. Upton, C. Ung, D.M.T. Yu, A. Ehteda, R. Pandher, C. Mayoh, S. Hebert, N. Jabado, C.L. Kleinman, M.R. Burns, M.D. Norris, M. Haber, M. Tsoli, D.S. Ziegler, Dual targeting of polyamine synthesis and uptake in diffuse intrinsic pontine gliomas, Nat. Commun. 12 (1) (2021) 971.
[55] J. Chen, H. Ni, Z. Meng, J. Wang, X. Huang, Y. Dong, C. Sun, Y. Zhang, L. Cui, J. Li, X. Jia, Q. Meng, C. Li, Supramolecular trap for catching polyamines in cells as an anti-tumor strategy, Nat. Commun. 10 (1) (2019) 3546.
[56] M.S. Goldberg, Improving cancer immunotherapy through nanotechnology, Nat. Rev. Cancer 19 (10) (2019) 587–602.